JOURNAL OF CATALYSIS 63, 201–216 (1980)

Structure of Oxide CoMo/γ-Al_2O_3 Hydrodesulfurization Catalysts: An XPS and DRS Study

P. GAJARDO, P. GRANGE, AND B. DELMON

Université Catholique de Louvain, Groupe de Physico-Chimie Minérale et de Catalyse, Place Croix du Sud, 1, 1348 Louvain-la-Neuve, Belgium

Received November 27, 1978; revised November 14, 1979

A series of CoMo/γ-Al_2O_3 oxide catalysts containing 15.0 ± 0.6 wt% of cobalt and molybdenum oxides (considered as Co_3O_4 and MoO_3) and r = Co/(Co + Mo) atomic composition ranging from 0.00 to 1.00 were studied by XPS and diffuse reflectance spectroscopy. These techniques and previously reported results on electron microscopy show that molybdenum occurs on γ-Al_2O_3 as tetrahedral oxidic Mo(VI) according to the Mo(VI) monolayer model, and also as Mo(VI) in multilayers having a bulk like MoO_3 or paramolybdate surrounding. Cobalt is poorly dispersed when alone (15%) on a γ-Al_2O_3 surface; in that case, the formation of Co_3O_4 clusters is extensive, and very little $CoAl_2O_4$ is formed. In the r = 0.25–0.75 composition range, a strong interaction takes place between molybdenum of the monolayer and cobalt, which brings about a high dispersion of cobalt and seems, in turn, to increase the dispersion of molybdenum. As a consequence of the dispersion of cobalt, much $CoAl_2O_4$ is formed. The results, as well as the properties of the catalysts in the middle range of composition r, are interpreted in terms of a model of the catalyst surface in which a bilayer of Co–Mo is formed on the $CoAl_2O_4$.

1. INTRODUCTION

Several models have been proposed for describing cobalt–molybdenum catalysts supported on γ-Al_2O_3 in their oxidic form, namely before they are subjected to activation and to the reacting conditions in hydrodesulfurization.

The main feature underlying these pictures is the extensive spreading of molybdenum oxide on the surface of alumina and the formation of a monolayer of molybdenum oxide (*1–3*) and of $Al_2(MoO_4)_3$ (*4*).

The situation is less clear when the interaction of cobalt with the support is considered. It has been reported that cobalt can be placed in tetrahedral (*5–7*) or in octahedral positions (*8*) or in both (*9*) on the alumina surface. The formation of some $CoAl_2O_4$ has been also observed (see, for example, (*10–12*).

When cobalt and molybdenum are simultaneously present on the support, the results reported in the literature yield a rather confusing picture. Schuit and Gates (*1*) detailed a model based on the existence of a Mo(VI) monolayer on the alumina surface, with cobalt(II) being located in the alumina superficial layers beneath the Mo(VI) monolayer. Using a substantially different approach, Grimblot *et al.* (*13, 14*) gave a detailed description of the surface species for the various composition ranges; in particular, they suggest the existence of a species associating four molybdenum ions with one of cobalt. On the other hand, the formation of $CoMoO_4$ on γ-Al_2O_3 has been mentioned by Gour *et at.* (*11*).

Discrepancies in the conceptions of the structure of CoMo/Al_2O_3 catalysts can be explained by the fact that different catalyst preparation methods were used and also because physicochemical methods usually employed only gave partial information about the catalyst characteristics.

In this work, we have made an attempt to elucidate the structure of a series of CoMo/γ-Al_2O_3 oxide catalysts, the behavior of which in reduction experiments was reported elsewhere (*15*). In this series, the catalyst compositions, expressed by the atomic ratio r = Co/(Co + Mo), change

0021-9517/80/050201-16$02.00/0

from 0.0 to 1.0, the total active phase content remaining constant.

We report here principally results of X-ray photoelectron spectrsocopy (XPS) and diffuse reflectance spectroscopy (DRS). In the discussion, we shall also recall the essential results obtained in a previous study using high-resolution electron microscopy (SEM and STEM) and high-resolution electron microprobe analysis (*16*).

2. EXPERIMENTAL METHODS

2.1. Reference Compounds

The preparation methods of MoO_3, Co_3O_4, and a-$CoMoO_4$ (green) were described in a previous paper (*15*).

$CoAl_2O_4$ was prepared by heating a mixture of $Co(NO_3)_2 \cdot 6H_2O$ with γ-Al_2O_3 at 1100°C for 48 hr. Before the high-temperature treatment, the mixture was progressively heated at 100°C for 4 hr and then at 300°C for 14 hr. X-Ray diffraction gave the typical spectrum of $CoAl_2O_4$.

Commercial $Na_2MoO_4 \cdot 2H_2O$, UCB (p.a.), and $(NH_4)_6Mo_7O_{24} \cdot 4H_2O$, (APM) Merck (p.a.), were used.

2.2 Catalysts

The catalysts are those previously studied in reduction experiments (*15*). They were prepared by double impregnation. Molybdenum was impregnated first and then, after catalyst calcination, cobalt. The details of the preparation method have already been described (*15*). Catalysts are designated by a symbol indicating the support, namely, Al (γ-Al_2O_3), followed by the approximative value of the ratio r = Co/(Co + Mo) (atomic); for example, Al-0.75 corresponds to $r = 0.75$. Weight content of supported oxides (Co_3O_4 + MoO_3) is 15.0 ± 0.6% of the total weight of the catalyst. The samples were in the form of fine powders.

Color, composition, and surface area of catalysts are reported in Table 1 (taken from Ref. (*15*)).

2.3. X-Ray Photoelectron Spectroscopy (XPS)

2.3.1. Equipment

The XPS equipment was a Vacuum Generator ESCA 2. The excitating radiation was Al$K\alpha$ ($h\nu$ = 1486.6 eV). The electrostatic analyzer energy was set at 90 eV. A Tracor Northern NS 560 signal averager was used to improve the signal-to-noise ratio. The samples were dusted onto double-sided adhesive tape and introduced into the preparation chamber. They were left there for a few minutes at room temperature under a vacuum of $\simeq 1 \times 10^{-6}$ Torr.

2.3.2. Recording, Decomposition of Spectra, and BE Determinations

The spectra of the C_{1s}, O_{1s}, Al_{2p}, Al_{2s},

TABLE 1

Color, Composition, and Surface Area of the CoMo/γ-Al_2O_3 Oxidic Catalysts (Table from (*15*))

Catalyst	Color	Percentage (wt) of oxide phases in the catalyst			Co: Co + Mo	Surface area ($m^2\ g^{-1}$)
		MoO_3	Co_3O_4	MoO_3 + Co_3O_4		
Al-0.00	White	14.80	0.00	14.80	0.00	109
Al-0.05	Light violaceous	13.97	0.45	14.42	0.05	152
Al-0.25	Gray-bluish	12.08	2.52	14.54	0.27	125
Al-0.35	Gray-bluish	10.86	3.82	14.68	0.38	123
Al-0.50	Gray-black	9.65	5.96	15.61	0.52	140
Al-0.75	Black	6.03	9.95	15.98	0.75	142
Al-1.00	Black	0.00	14.46	14.46	1.00	111

$Mo_{3d_{5/2}}$, $Mo_{3d_{3/2}}$, and $Co_{2p_{3/2}}$ levels were recorded. The order of recording was the same for all catalysts. The reference line was $Au_{4f_{7/2}}$ (binding energy, BE, = 82.8 eV). It was found that the BE of O_{1s} and Al_{2s} levels is independent of the catalyst composition; consequently these lines were also used as references in the determination of the BE of Mo_{3d} Co_{2p}. The advantages of the use of the Al_{2s} and O_{1s} as reference lines have been reported by Ogilvie and Wolberg (*17*). The BE of internal references (O_{1s} and Al_{2s}) was the average value of BE calculated from all catalysts taking as reference $Au_{4f_{7/2}}$ line. Considering that intensity of signal and resolution of our apparatus often decrease after gold deposition, spectra were recorded before and after gold evaporation. Thus, BE of Co_{2p} and Mo_{3d} levels was also determined before gold deposition, using the internal references. The estimated accuracy which can be obtained with our equipment, using internal reference, is ±0.3 eV. In order to reduce the error associated with carbon contamination and charging of the sample, the number of scans per spectrum was limited to a minimum, enough to decompose the spectrum.

The decomposition of the spectra into their components was performed on an IBM computer, using a special program. In one computer program, the background produced by the inelastically scattered electrons was assumed to increase linearly with the BE. In another program, the background shape was assumed to be adequately reproduced by the normalized integral of background-free peak. The mean standard deviation between the experimental curve and the theoretical one, corresponding to the decomposition of the spectra by the computer, is lower with the former method; accordingly, we used it throughout this work.

The following hypotheses or constraints, consistent with literature data, have been chosen in the decomposition of spectra: (i) the shape of the line is gaussian in all studied spectra (this is the case, with a 95% accuracy, with the equipment used, as shown by computer decomposition); (ii) the $Mo_{3d_{5/2}}$ and $Mo_{3d_{3/2}}$ peaks have the same full width at half-maximum (FWHM) (*18*); (iii) the maxima of these lines are separated by 3.2 eV; and (iv) the ratio of their intensities ($Mo_{3d_{5/2}} : Mo_{3d_{3/2}}$) is 1.54. These two last values have been determined experimentally from pure MoO_3; the intensity ratio is higher than the theoretical one [≃1.46, calculated from the theoretical photoionization cross sections (*19*)]. The spectrum of the $Co_{3p_{3/2}}$ level was decomposed into only one peak and one satellite, placed on the high BE side. This decomposition is sufficient, in view of the shape of the line, and corresponds to literature information (*20, 21*). A decomposition in several peaks would be highly speculative with our apparatus.

2.3.3. Quantitative Chemical Analysis

In order to perform quantitative XPS analyses, we take as line intensity the area under the gaussian curve. To facilitate this task, we take as line intensities of Mo the sum of intensities of $Mo_{3d_{5/2}}$ and $Mo_{3d_{3/2}}$ peaks; in the case of cobalt, the intensity was the sum of intensities of $Co_{2p_{3/2}}$ and satellite peaks. Then, using response coefficients of the apparatus, we transform these intensities to their corresponding atomic intensities, which are proportional to the number of atoms "seen" by XPS. The atomic intensities are designated in this study as I_x, where x represents the studied element. Thus, the atomic intensities for Mo, Co, and Al are I_{Mo}, I_{Co}, and I_{Al}, respectively.

The response coefficient of the apparatus is calculated for each studied element by experimental calibration using for this purpose model compounds having at least one common ion. The model substances used in the calibrations were a-$CoMoO_4$, $CoAl_2O_4$, $Na_4(SiMo_{12}O_{40})$, and $CoSO_4$. These model compounds were chosen taking into account their stability at the conditions of

XPS analysis and their possible presence in the catalyst. We expected thus, to diminish side problems, like transformation of the surface compounds during analysis and the possible influence of the matrix of solid on the signal intensity.

The continuous contamination of the sample surface observed when the analysis is in progress is a considerable problem in XPS quantitative measurements. This contamination brings about an inescapable and continuous decrease of the XPS signal intensities. Therefore, in order to obtain reproducible results, a strict standardization of the order of recording is required. We have estimated that the relative error due to contamination is no more than 15% if the standardized procedure is used.

In this work, the amount of ions detected by XPS is expressed as fraction of atomic intensities of studied elements. For instance, if Mo, Co, and Al are the elements considered, the fraction of atomic intensity of cobalt is $I_{Co}/(I_{Co} + I_{Mo} + I_{Al})$, which really corresponds to the *atomic fraction* of Co, Mo, and Al *"seen" by XPS.*

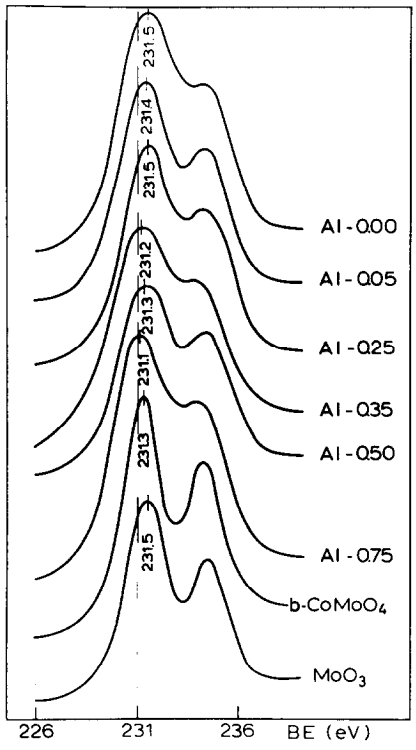

FIG. 1. XPS spectra of Mo_{3d} levels of catalysts and unsupported model compounds.

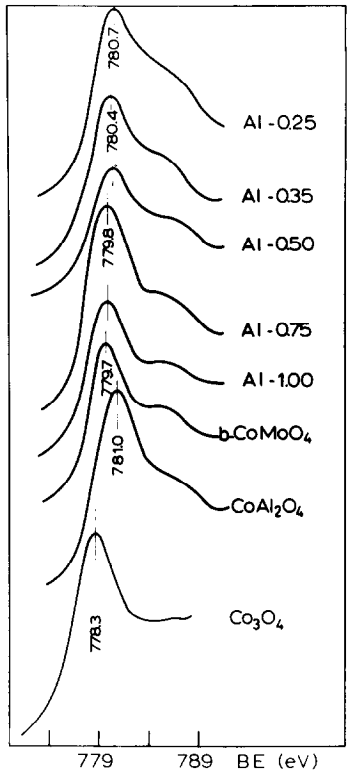

FIG. 2. XPS spectra of $Co_{2p_{3/2}}$ level of catalysts and unsupported model compounds.

2.4. Diffuse Reflectance Spectroscopy

Spectra (200–1840 nm) of catalysts were recorded using a Beckman ACTA MIV spectrophotometer. A pellet of the pure catalyst support (γ-Al_2O_3) was used as reference. Pellets of catalyst and reference were obtained by powder pressing at 1.7 tons/cm².

3. RESULTS

3.1 XPS

3.1.1. Spectra

Figures 1 and 2 present the spectra of

Mo_{3d} doublet and the $Co_{2p_{3/2}}$ line obtained from catalysts and model compounds.

3.1.2. *Exploitation of Data Concerning Cobalt*

In studies of cobalt oxides, the ratio between the intensity of the $Co_{2p_{3/2}}$ line, I_p, and the sum of intensities of I_p and its satellite, I_s $[I_p/(I_p + I_s)]$, can be used to identify the presence of high-spin Co(II) and of Co_3O_4 on the surfaces (*14, 20, 21*). We have plotted $I_p/(I_p + I_s)$ on Fig. 3a against the atomic composition of the catalyst. Figure 3a indicates an increase of the species characterized by high $I_p/(I_p + I_s)$ ratio with increasing r.

We have also attempted to detect variations of the BE of the cobalt species. The small amounts of cobalt present on the catalyst, the charge effect linked to the low electrical conductivity of the catalysts and the moderate resolution of the spectra, introduce some uncertainties in the BE determination of the $Co_{2p_{3/2}}$ level. Therefore, the determination of the BE of Co_{2p} was repeated at least twice. Figures 3b and c are plots of the corresponding results against catalyst composition, taking respectively O_{1s} and Al_{2s} as references.

3.1.3. *Intensities*

In order to gain some information on the distribution of cobalt and molybdenum on the alumina support, we measured the intensities of the peaks corresponding to the $Co_{2p_{3/2}}$, Mo_{3d}, and Al_{2p} levels (I_{Co}, I_{Mo}, and I_{Al}, respectively). In trying to compare the variations of the intensities of the peaks, we assumed that they are affected to the same degree by the presence of oxygen atoms in the oxides and by the carbon present on the catalyst surface. Figures 4a and b are the plots of $I_{Al}/(I_{Al} + I_{Co} + I_{Mo})$, $I_{Mo}/(I_{Al} + I_{Co} + I_{Mo})$, and $I_{Co}/(I_{Al} + I_{Co} + I_{Mo})$ vs atomic composition of the catalysts. A minimum in the Al_{2p} line is observed for $0.25 < r < 0.75$; this corresponds to a modest maximum of Mo_{3d} and a quite conspicuous maximum of Co_{2p}.

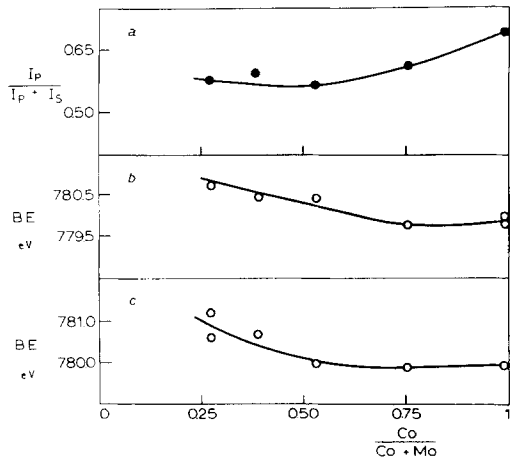

FIG. 3. $I_p/(I_p + I_s)$ and BE dependencies of $Co_{2p_{3/2}}$ level on atomic composition of catalysts.

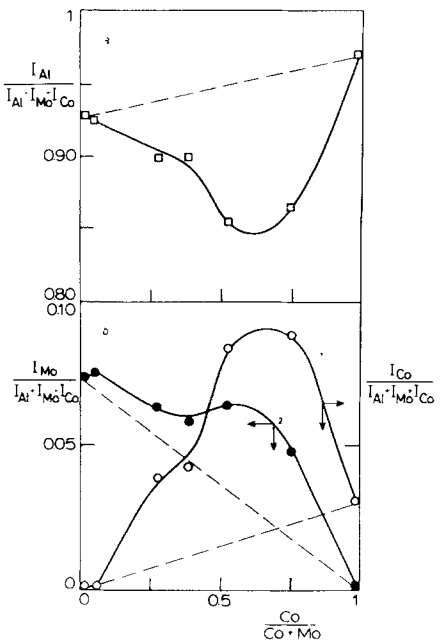

FIG. 4. Dispersion of Co and Mo on the catalyst surfaces.

3.2 Diffuse Reflectance Spectra

The spectra of the catalysts and of model compounds (Co_3O_4, $CoAl_2O_4$, MoO_3, $Na_2MoO_4 \cdot 2H_2O$), ammonium paramolybdate (APM), and a-$CoMoO_4$ are presented in Fig. 5 (200–800 nm) and Fig. 6 (800–1840 nm).

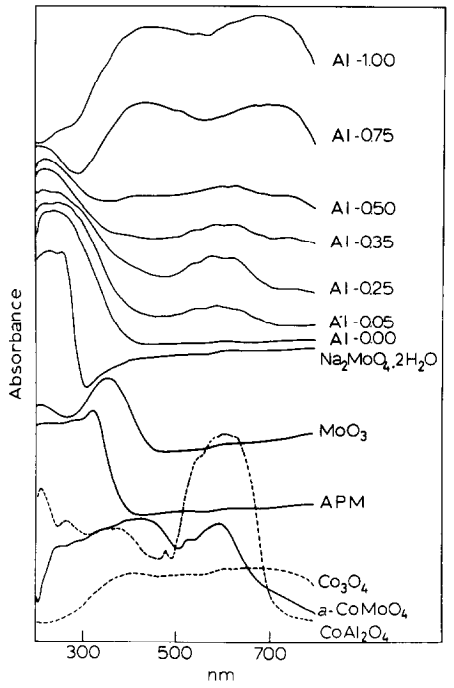

FIG. 5. Diffuse reflectance spectra of catalysts and unsupported model compounds.

4. DISCUSSION

4.1. XPS RESULTS

4.1.1. Identification of Surface Species

Comparing the Mo_{3d} spectra of the catalysts and those of the model compounds (Fig. 1) and their BE values, we can assume that most of the Mo is present as Mo(VI) in oxidic surroundings. Nevertheless, a conspicuous fact is the broadening of the Mo_{3d} doublet. We do not believe that the poor separation of the doublet should be attributed to our apparatus and measurement conditions, carbon deposition, and charging effect, as this doublet is well separated in unsupported a-$CoMoO_4$ and MoO_3 (Fig. 1) and the broadening appears even when only one scan is performed. This poor separation rather suggests the simultaneous existence of several molybdenum oxidic species on the surface of the support, having slightly different binding energy values. One of these species is probably the Mo(VI) monolayer, whose presence is generally accepted in this kind of catalyst. the easy formation of this monolayer on the Al_2O_3 surface (*1–3*) suggests that there should be a rather strong interaction between the alumina surface and Mo(VI) (*22*).

Mo(V) can also be present on such catalysts contributing to a broadening of the Mo_{2d} doublet. Indeed, this ion has been detected (actually in very low concentration) by ESR on Mo/γ-Al_2O_3 oxide catalysts prepared by the same method (*23, 24*). Some Mo(V) could also be formed even during XPS measurements. The presence of Mo(V) would correspond to a shift in the BE toward lower values.

Finally, as we will see in Section 4.2.1, at high Mo loading, when Mo(VI) monolayer is completed, besides a polymolybdate form, the excess of Mo could form bulk MoO_3 or a multilayer of MoO_3-like species. The coexistence of these species in one catalyst could also contribute to the broadening of the Mo_{3d} doublet.

Concerning cobalt, the spectra of the $Co_{2p_{3/2}}$ level also exhibit some broadening (Fig. 2). This can be explained by the exchange interaction between the unpaired

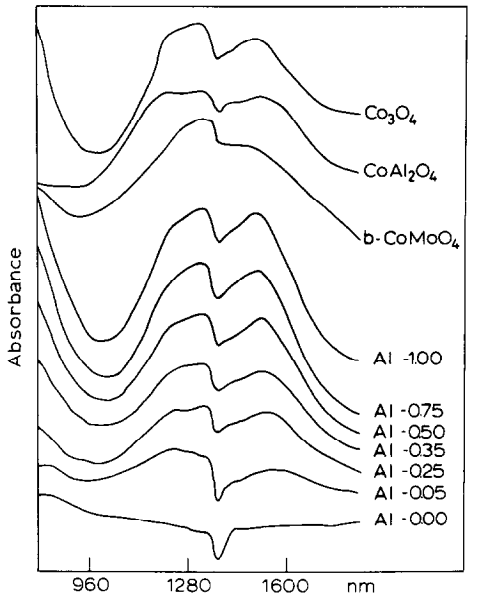

FIG. 6. Diffuse reflectance spectra of catalysts and unsupported model compounds.

valence electrons and those of the 2*p* level (*12, 20*) and/or by the simultaneous presence of the Co(II) in octahedral and tetrahedral surroundings having similar BE (*25*).

XPS measurements yield two kinds of information concerning cobalt species, namely, BE and intensity of the satellite of the $Co_{2p_{3/2}}$ line relative to the intensity of the main peak. As the precision of both measurements is relatively poor, a careful comparison with the spectra of model compounds will be used to support the interpretations.

In the case of cobalt compounds, a correlation has been shown to exist between the paramagnetic properties of cobalt and the intensity of the $Co_{2p_{3/2}}$ "shake-up" satellite; this correlation has been illustrated by Borod'ko *et al.* (*21*). The higher the effective magnetic moment, the higher the intensity of the $Co_{2p_{3/2}}$ satellite. Let us consider the model compounds $CoAl_2O_4$, a-$CoMoO_4$, and Co_3O_4. In the first two compounds, cobalt is present as Co(II). The BE values are 781.0 eV for $CoAl_2O_4$ and 779.7 eV for a-$CoMoO_4$. Both compounds have a prominent shake-up satellite, with $I_p/(I_p + I_s)$ ratios of 0.58 and 0.57, respectively. In Co_3O_4, tetrahedral Co(II) and octahedral Co(III) are present in the proportion 1 : 2; Co(III), being diamagnetic, has no satellite (*19, 20*). The corresponding BE is 778.3 eV and $I_p/(I_p + I_s)$ equals 0.82.

In our catalysts, the $I_p/(I_p + I_s)$ ratio increases with augmentation of the cobalt content, whereas the BE of the $Co_{3p_{3/2}}$ level decreases (Figs. 3a and b). This indicates an increase of the contribution of Co(III); this fact strongly suggests the existence of Co_3O_4 in Al-0.75 and Al-1.00. However, the contribution of the paramagnetic cobalt species remains important even in the Al-1.00 catalyst ($I_p/(I_p + I_s) \simeq 0.7$ compared with 0.82 for Co_3O_4); in addition, the $Co_{2p_{3/2}}$ BE value is far from that of Co_3O_4. This indicates that another paramagnetic Co species is present besides Co_3O_4. The spectra of the $Co_{2p_{3/2}}$ line (Fig. 2) and the results shown in Figs. 3a and b strongly suggest the presence of Co(II) species (compare the characteristics of these catalysts with those of the $CoAl_2O_4$ and a-$CoMoO_4$). XPS alone is not able to give more precise information; in Section 4.3.2 we will discuss this question putting together DRS and XPS results.

4.1.2. Distribution of the Cobalt and Molybdenum on the Support

XPS is a good tool in studies of the dispersion of metals on supports (see Ref. (*26–28*)). However, there are some difficulties in this kind of study (*28–30*) such as a diffusion of metal ions into the support, a heterogeneous distribution of the metal on the support, and the inescapable polydispersity of the metal particles (if λ is the mean free path of the analyzed electrons and d is the thickenss of the metal crystallite, λ/d varies from crystallite to crystallite).

In spite of these limitations, valuable estimations of ion distribution on support can be obtained if a proper calibration of apparatus and a strict control of contamination are achieved. In addition, these difficulties are less critical if a series of catalysts, prepared by the same method, with the same materials, are comparatively studied and only one single parameter is changed continuously. This is the case of our catalyst series and the variable parameter is the r = Co/(Co + Mo) ratio (Figs. 4a b).

In our CoMo/γ-Al_2O_3 catalysts, molybdenum was deposited first on the γ-Al_2O_3 and then cobalt. As the XPS signals come from a depth of 10–30 Å (*31*), they give a statistical composition of the corresponding subsurface domains (the composition of which might not be constant with depth). As the total active phase content (Co_3O_4 + MoO_3) is the same in all catalysts, a decrease of the XPS signal of one of the metal ions (cobalt or molybdenum) can have one of the following causes: (i) a reduction of the total amount of the referred metal ion, i.e., changes in the r = Co/(Co + Mo)

ratio; (ii) a decrease of its dispersion on the surface; (iii) an overlying of it by layers of the second metal ion (or a dissolution in this layer); (iv) a migration of the referred metal ion into the support. On the other hand, a decrease of the Al_{2p} signal indicates that the support is covered by cobalt and/or molybdenum ions.

The dashed line in Fig. 4a corresponds to the theoretical $I_{Al}/(I_{Al} + I_{Co} + I_{Mo})$ value which would be observed if cobalt and molybdenum would retain the same state of dispersion as they have in Al-0.00 and Al-1.00 catlaysts. The $I_{Al}/(I_{Al} + I_{Co} + I_{Mo})$ value reaches a minimum when the composition of the catalyst is about $r = 0.50$ (Fig. 4a). This means that the uncovered or not heavily covered γ-Al_2O_3 surface increases and, therefore, that the dispersion of cobalt or molybdenum or both decreases when catalysts become richer in cobalt or in molybdenum.

Figure 4b gives $I_{Co}/(I_{Al} + I_{Co} + I_{Mo})$ (curve 1) and $I_{Mo}/(I_{Al} + I_{Co} + I_{Mo})$ (curve 2); the dashed lines have the same significance as in Fig. 4a. The curve corresponding to Co indicates that this element is poorly dispersed when it is present alone on γ-Al_2O_3.

The spreading of Co on the surface is dramatically augmented if some molybdenum oxide is present on γ-Al_2O_3. Actually, in catalyst Al-1.00, only 3% of all atoms detected by XPS corresponds to cobalt atoms (see Fig. 4b, curve 1, at Co/(Co + Mo) = 1.00). This percentage becomes almost three times higher in catalyst Al-0.75, in spite of the fact that the overall cobalt content in this latter catalyst is 25% lower than in the former. In neither case did we observe the formation of compounds like $CoAl_2O_4$ or $CoMoO_4$ (see below). This indicates the absence of any significant migration of cobalt into the support of Al-0.75 and Al-1.00 catalysts. Considering catalyst Al-0.50 as a reference, the drop of curve 1 (Fig. 4b), observed when r diminishes, can be attributed mainly to the decrease of the total content of cobalt, supposing an almost constant dispersion. However, the decrease is slightly more abrupt than expected. This would suggest the penetration of increasing proportions of cobalt into γ-Al_2O_3 [in this catalyst the formation of the $CoAl_2O_4$ has been detected by DRS (see later)]

The enhancing effect of molybdenum on cobalt dispersion can be explained in terms of a strong interaction taking place between both ions on the surface of the carrier. Actually, if molybdenum remains strongly attached to γ-Al_2O_3, forming a Mo(VI) monolayer, the presence of forces linking cobalt to molybdenum monolayer could bring about a cobalt dispersion on the surface. Nevertheless, these forces must be sufficiently weak as not to detach the molybdenum from the γ-Al_2O_3 surface and thus to form $CoMoO_4$. This last phenomenon could take place in a support like SiO_2, where Mo is weakly attached to support and where the formation of $CoMoO_4$ is observed.

Comparing Al-0.00 and Al-1.00, one notices that molybdenum is more dispersed than cobalt on γ-Al_2O_3. Indeed, $\simeq$7.5% of all atoms detected by XPS corresponds to molybdenum atoms (see Fig. 4b, curve 2, at Co/(Co + Mo) = 0.00). This is logical, in view of the tendency of molybdenum to spread in the form of a monolayer (*1–3*). A new and more surprising fact is the increase of the dispersion of molybdenum when r increases. Martinez *et al.* (*32*), using reflectance spectroscopy, observed the same phenomenon. When trying to interpret this effect, it is not necessary to suppose that the dispersion of molybdenum is increased when cobalt is present. The same variation would be observed if a more or less constant fraction of the surface was covered by a monolayer of molybdenum in the $0.00 < r < 0.50$ range, with the decrease of the bulklike MoO_3 [whose presence in these catalysts has been detected (see Section 4.2.1)], the contribution of which to XPS signals is presumably smaller. It is worth to notice that the atomic fraction of

surface cobalt as seen by the XPS is higher than that of molybdenum in the catalyst having $r \geq 0.50$.

4.2. Diffuse Reflectance Spectra

4.2.1. Molybdenum species

DRS is quite suitable for the identification of the coordination symmetry of the Mo(VI) on the surface of catalysts if a careful comparison is made with the spectra of typical compounds either in tetrahedral oxidic environment ($Na_2MoO_4 \cdot 2H_2O$) or in octahedral oxidic environment (MoO_3, AMP, and a-$CoMoO_4$) (*5, 9, 33, 34*).

According to the preparation method employed in this work, XPS results, and literature data, most of molybdenum ions in our catalysts must be in the 6+ oxidation state. Consequently, 6+ will be the only oxidation state considered in the attribution of the absorption bands of the catalyst in Fig. 5.

There is a strong broad absorption band whose maximum is situated between 200 and 300 nm. Its relative intensity diminishes with increasing cobalt content. According to literature, the bands of octahedral and tetrahedral oxidic forms of Mo(VI) appear in this region of the spectrum (charge transfer transitions), namely, octahedral at 290–330 nm, tetrahedral at 250–280 nm, and both octahedral and tetrahedral at 225–240 nm (*9, 33, 35*). This is corroborated by spectra of our model compounds, where Mo(VI) is situated in tetrahedral ($Na_2MoO_4 \cdot 2H_2O$) and octahedral (or near octahedral) surroundings (AMP and MoO_3) (in our case the maximum for MoO_3 is slightly shifted to the high wavelength side). In the catalysts, the maxima of the absorption bands are clearly situated between 200 and 280 nm; this fact indicates the presence of tetrahedral Mo(VI) (compare Al-0.00 and $Na_2MoO_4 \cdot 2H_2O$ spectra). However, these bands are broader than expected. This suggests that Mo(VI) in octahedral and/or distorted octahedral coordination is also present in the catalysts. Indeed, the beginning of this band (on the high wavelength side) lies between 300 and 400 nm, which corresponds to the position of the absorption band of Mo(VI) close to octahedral environment (compare spectra of Al-0.00, MoO_3, and APM, Fig. 5). Considering that the bands of Al-0.00 and APM begin at nearly the same position ($\simeq$400 nm), it is reasonable to conclude that, in our catalysts, the major part of Mo(VI) is situated in tetrahedral position and a smaller part is present in a polymolybdate or bulklike MoO_3 environment. These results are well supported by previously reported results (*9, 32–34*). In particular Praliaud and Giordano *et al.* pointed out that the relative quantities of the tetrahedral and octahedral Mo(VI) depend on catalyst preparation method, molybdenum content, and calcination temperature. The higher the molybdenum content and the calcination temperature, the higher the amount of octahedral Mo(VI). Giordano *et al.* have proposed that the tetrahedral Mo(VI) absorption band comes from the structure

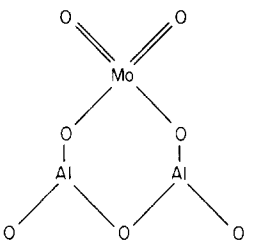

This structure would be present on alumina surface at low molybdenum content and at relative low calcination temperatures (<500°C). This is in agreement with the mechanism of formation of Mo(VI) structure adsorbed on alumina proposed by Dufaux *et al.* (*36*) and with Hall's model of the Mo(VI) monolayer. Giordano *et al.* indicate that these tetrahedral Mo(VI) structures begin progressively to condense in polymeric forms, leading to octahedral polymeric forms of Mo(VI) adsorbed on Al_2O_3, when the catalyst becomes richer in

molybdenum and when the calcination temperature is higher. Thus, at high Mo loading the occupancy of the octahedral sites of Al_2O_3 would be an alternative way for the formation of octahedral Mo(VI).

We think that our results can basically be interpreted according to Hall's monolayer model, where the Mo(VI) is in tetrahedral oxidic surrounding, and Giordano's polymeric model, in spite of the fact that our alumina (160 m^2 g^{-1}) could theoretically accommodate 15–18% of MoO_3 as a monolayer (the maximum loading of MoO_3 in the catalyst is 14.8%). We can assume that at high Mo loading, besides Mo placed in some octahedral sites of γ-Al_2O_3, octahedral Mo(VI) comes from octahedral Mo(VI) placed in multilayers deposited on the Mo(VI) monolayer. In this multilayer structure, Mo(VI) would have an environment similar to that in MoO_3 or in polymolybdates. The actual formation of such aggregates, thicker than a molybdenum monolayer, in our catalysts is supported by the following facts: (i) the presence of such molybdenum aggregates in our catalyst is deduced from ESCA (Fig. 4a, curve 2); (ii) the addition of small amounts of cobalt (for example in the Al-0.05 catalyst) enhances the reduction by hydrogen of this type of catalyst, which is characteristic of the behavior of bulk MoO_3 (*15*); (iii) from the literature it is known that the presence of such an octahedral Mo(VI) is possible in a catalyst having a high molybdenum content (*34–36*).

4.2.2. *Cobalt Species*

The broad triple band situated between 500 and 700 nm is due to ligand field transitions of tetrahedral Co(II) (*9, 37–39*); it can be unambiguously assigned to tetradedral Co(II) in $CoAl_2O_4$ (compare spectra of our catalysts and of $CoAl_2O_4$, Fig. 5). The intensity of this band (relative to the Mo(VI) bands) increases when the cobalt content decreases. This is a quite surprising phenomenon. In catalysts where the presence of Co_3O_4 has been observed (r = 0.75–1.00), the decreasing of the intensity of 500 to 700-nm bands of $CoAl_2O_4$ may be merely explained by an "obscuring effect" of this band resulting from the superposition of strong bands of Co_3O_4 (700–300 nm) (see later). In catalysts with r = 0.05–0.5, where Co_3O_4 has not been observed by XPS, AEM, and H_2 reduction (*15*), the increasing of the 500 to 700-nm band may be reasonably explained by a real increase in the amount of $CoAl_2O_4$ in the catalyst (observed when r diminishes) rather than by an "obscuring effect" of Co_3O_4 bands.

Indeed, recalling the results of the XPS measurements, where it was shown that Mo(VI) promotes the dispersion of cobalt, we can assume that Mo(VI) also promotes the formation of $CoAl_2O_4$. Thus, it is quite logical that the penetration of cobalt into γ-Al_2O_3 and the formation of $CoAl_2O_4$ spinel are favored by a better dispersion of cobalt on the support, namely by an augmentation of the contact area between cobalt and the Mo–Al_2O_3 surface. Because of dispersion of cobalt alone on γ-Al_2O_3 (i.e., Al-1.00 catalyst) is low, the formation of $CoAl_2O_4$ is quite restricted in the catalyst with high cobalt loading.

The Mo(VI) monolayer could promote the formation of $CoAl_2O_4$ not only by increasing the dispersion of cobalt, but also by a chemical effect; a ternary Co–Mo–Al_2O_3 surface species being energetically more favorable could be formed. According to the monolayer model elaborated by Schuit and Gates, the penetration of cobalt into γ-Al_2O_3 (beneath Mo(VI) monolayer) stabilizes this monolayer, expulsing Al^{3+} ions from support to the surface. Lo Jacono *et al.* (*37*) have proposed that Mo(VI)–Al_2O_3 complex favors the placing of cobalt ions in its vicinity, forming a spinel-like structure with the Al_2O_3.

In order to identify other cobalt species present in the catalyst, let us compare the absorption bands of model compounds containing cobalt and those of the catalysts. From Figs. 5 and 6, we can deduce that

besides tetrahedral Co(II), cobalt is also present in octahedral Co(III) in oxidic surrounding. Indeed, the spectra of Co_3O_4 and of the catalysts present the following common bands which had been assigned to octahedral Co(III): (i) the absorption band at $\simeq$400 nm (*9, 37, 39, 40*); (ii) the absorption band in the range 650–960 nm, having an absorption maximum at $\simeq$700 nm (*37, 39, 40*). This band comes out cleanly in the Al-0.75 and Al-1.00 catalysts, but the strong triple band of $CoAl_2O_4$ (at $\simeq$600 nm) becomes superposed to it in catalysts with $r < 0.5$. In this case, the large 650 to 960-nm absorption band forms a shoulder (not indicated in our figures because it appears at the end of this spectrum of Fig. 5 and at the beginning of the spectrum of Fig. 6), also observed by Lo Jacono *et al.* (*37*) and El'bert and Tryasunov (*38*). Lo Jacono attributed it to the presence of the Co_3O_4 and El'bert to isolated Co(III); (iii) the bands appearing in the range 1000–1840 nm can be assigned to both octahedral Co(III) and tetrahedral Co(II) in $CoAl_2O_4$ surrounding. Actually, absorption bands of $CoAl_2O_4$ and Co_3O_4 are quite similar in this range.

There is no evidence, in the spectra of Figs. 5 and 6, of the presence of octahedral Co(II); nevertheless, it is not possible to exclude the existence of this species. Actually, if both tetrahedral and octahedral Co(II) occur together on the catalyst, the stronger band of tetrahedral cobalt will cover the weaker bands of octahedral cobalt (*9*).

In the cases of Al-1.00 and Al-0.75, the assignment of the Co(III) bands is well corroborated by XPS and previous results of gravimetric reduction obtained on the same series of catalysts (*15*), which indicated the presence of Co_3O_4 in these solids. A difficulty in ascribing the Co(III) bands remains however, as in the other catalysts (r = 0.05–0.50), we could not detect Co_3O_4 neither in reduction experiments nor from the BE and $I_p/(I_p + I_s)$ values in XPS measurements. We shall propose explanation in the next section.

4.3. General Picture of the Oxidic $CoMo/\gamma\text{-}Al_2O_3$ Catalysts

Putting together the conclusions of the two previous sections and those of the electron microscopy and electron microprobe analysis studies (*16*), we are in a position to propose a picture of the oxidic precursor of $CoMo/\gamma\text{-}Al_2O_3$ catalysts.

4.3.1. Summary of the Measurements in Electron Microscopy and Electron Microprobe Analysis

Let us first recall the results of electron microscopy and electron microprobe analysis (*16*). Physicochemical methods such as XPS and DRS give only an overall or averaged picture of the sample. In contrast, electron microscopy (SEM, STEM) and electron microprobe analysis (EMPA), having a good resolution, permit the study of the details of the texture of the sample, to estimate the distribution of the species on the catalysts, and to analyze the different domains present in the solid.

It was possible to differentiate three kinds of domains in the SEM, STEM, and EMPA observations of catalysts of our series:

(a) Domains characterized by aggregates containing cobalt oxide. The aggregates are present in all catalysts containing cobalt and are particularly important in Al-1.00. In catalysts with $r < 0.75$, the amount of such aggregates is very low; their existence is merely accidental. It was not possible to detect the existence of Co_3O_4 by gravimetric measurements of reduction by hydrogen for $r < 0.75$ (*15*). These aggregates have a crystalline structure; electron diffraction shows the typical pattern of Co_3O_4.

(b) Molybdenum–calcium aggregates, where crystallites of $CaMoO_4$ were indicated by electron diffraction. In our system, the amount of such crystallites is low and seems to be associated with Ca impurities.

(c) Domains where neither aggregates nor crystallites is observed, but where we can find cobalt and molybdenum. The

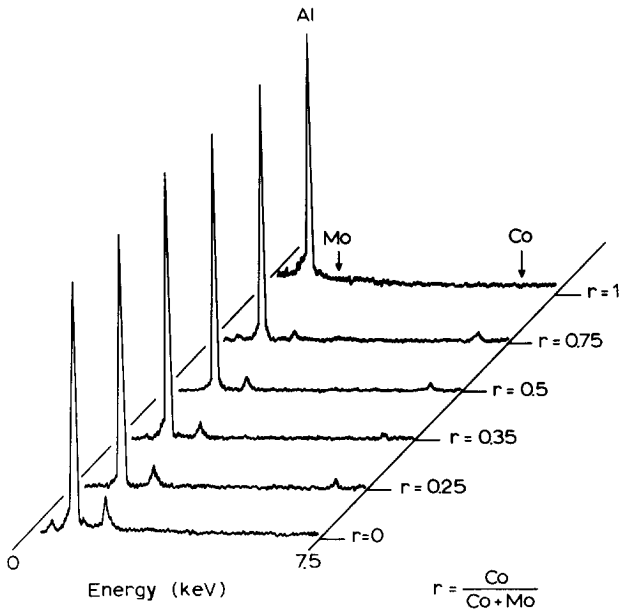

FIG. 7. Electron microprobe analysis (EMPA) of the "dispersed" zone of catalysts (taken from Ref. (*16*).

results of the chemical analysis of these domains, obtained by electron microprobe, are reported in Fig. 7, taken from Ref. (*16*). This figure indicates that the dispersed cobalt exists only if molybdenum is present in a dispersed state.

4.3.2. Co–Mo Bilayer Model of the Oxidic $CoMo/\gamma$-Al_2O_3 Catalyst

The existence of the molybdenum monolayer in Mo/Al_2O_3 catalyst is well documented (*1*, *3*) and is confirmed by our XPS and AEM results. The assumption that the Mo(VI) occupies the tetrahedral sites of the alumina at low and moderate Mo loading is based on the DRS spectra.

Reported XPS and AEM results on $CoMo/\gamma$-Al_2O_3 catalysts suggest a very good dispersion of both cobalt and molybdenum on the surface. These dispersed cobalt and molybdenum phases represent the major part of the cobalt and molybdenum content of the catalyst. Because of their large surface area, when they are present simultaneously, these phases are responsible for the signals obtained by XPS and DRS methods. On the other hand, Fig. 4 indicates that the cobalt atomic fraction "seen" by the XPS is higher than that of Mo at $r = 0.5$. For this catalyst composition, part of the cobalt is dissolved on the Al_2O_3 forming $CoAl_2O_4$. In contrast, Mo remains at the surface forming a monolayer. Therefore, if the amount of Co ions seen by XPS is higher than Mo ions, it is highly probable that at least part of Co is not placed under molybdenum, but rather *on* it forming a Co–Mo bilayer. Discrimination of the analysis due to differences in λ_{Mo} and λ_{Co} cannot explain this fact. Indeed, due to $\lambda_{Mo} > \lambda_{Co}$, the amount of Mo seen by XPS might be even higher than cobalt, in the ideal case when the analyzed sample is an homogeneous solution of Co, Mo, and Al_2O_3.

DRS results suggest that at least part of the Co in the bilayer is Co(III) in octahedral oxide surrounding (the existence of Co(II) in octahedral interstices is not excluded). Indeed the presence of such ions is observed in *all* catalysts containing cobalt. We must remark that in the case of $r = 0.05$–0.50 catalysts, the signal ascribed to octahedral Co(III) cannot be attributed to

Co_3O_4, because such a compound was not detected in these catalysts (*15*). The existence of octahedral Co(III) contradicts the XPS results. In effect, if this octahedral Co(III) exists on top of the Mo(VI) monolayer in its low-spin configuration (as in Co_3O_4), BE and $I_p/(I_p + I_s)$ values of $Co_{2p_{3/2}}$ line (Fig. 3) should be similar to that of Co_3O_4 and not similar to that of Co(II) as is really observed. This contradiction can be merely explained considering the existence of a slight reduction power of the XPS apparatus as it was observed on unsupported Co_3O_4 (*41*). Thus, if Co(III) is present before XPS analysis, it can be transformed into Co(II) during analysis. This could also explain the high proportion of Co(II) observed in the Al-1.00 catalyst in spite of the fact that great amounts of Co_3O_4 were detected in this catalyst by reduction measurements (*15*).

Taking into account the reported experimental results, we may conclude that dispersed cobalt and molybdenum form a "bilayer" on the $CoAl_2O_4$, cobalt being situated on the top of the Mo(VI) monolayer as octahedral Co(III) and Mo(VI) being located as Mo(VI) in the tetrahedral sites of the $CoAl_2O_4$ surface.

4.3.3. Experimental Evidences, Taken from Literature, Supporting a Bilayer Model of Co–Mo/γ-Al_2O_3 Catalyst

We will now report some important results obtained by other workers which can be explained by the proposed bilayer model of oxidic $CoMo/\gamma$-Al_2O_3 catalysts.

Moné (*42*) has reported experimental evidences for the existence of a "cobalt molybdate" configuration which can be well assimilated to our "Co–Mo bilayer." Actually, this author pointed out, by ir and DRS, the formation of a Lewis site band in the ir spectrum at 1612 cm^{-1} resulting from a cobalt–molybdenum monolayer interaction and, concomitantly, the formation of the $CoAl_2O_4$. In this case, the cobalt fraction remaining on the surface forming a "cobalt molybdate" configuration would depend on the calcination temperature. According to this author, Co occupies a "top" position in such a configuration. He observed the same phenomenon in the Ni–Mo/γ-Al_2O_3 catalysts.

Interaction between cobalt and molybdenum was observed by Ishii *et al.* (*43*) using a MoO_3 extraction method. These authors detected the formation of some mixed cobalt molybdenum oxide on $CoMo/\gamma$-Al_2O_3 catalysts which seems to be different from the unsupported $CoO–MoO_3$ catalyst.

Grimblot *et al.* (*13, 14*) have reported the presence of the "$CoMo_4$" phases in the $CoMo/\gamma$-Al_2O_3 catalysts by reduction gravimetric and XPS measurements.

Recently, Okamoto *et al.* (*44*), using the same kind of catalysts employed in this work, observed by XPS a stabilization effect of cobalt on molybdenum. Thus, cobalt forbids the molybdenum migration in $CoMo/\gamma$-Al_2O_3 catalysts during the hydrodesulphurization of thiophene performed at 400°C.

The enchancing effect of cobalt on the dispersion of molybdenum observed on $CoMo/\gamma$-Al_2O_3 catalysts by Martinez *et al.* (*32*) may account for a mutual action between both ions on the surface carrier.

The cobalt–molybdenum interaction on the Al_2O_3 has been mentioned by Brown *et al.* (*45*). These authors, using Raman spectroscopy, pointed out the presence of two bands (941 and 952 cm^{-1}) in $CoMo/\gamma$-Al_2O_3, which are also present in b-$CoMoO_4$ but absent in Mo/Al_2O_3 and Co/Al_2O_3. In our opinion, this suggests the presence of Co–Mo interactions in the catalysts, as it is observed in b-$CoMoO_4$ which may be interpreted in terms of a Co–Mo bilayer. These authors indicated that cobalt interacts with molybdenum via terminal oxygen–molybdenum bonds (1006 cm^{-1}). This last fact supports the hypothesis of the "top" position of cobalt on molybdenum monolayer.

The anomalous decrease of the hydrogen reducibility previously (*15*) observed on the same catalysts used in this work (at r = 0.25–0.50) may also be due to this Co–Mo

interaction taking place in the Co–Mo "bilayer."

4.3.4. *Species Present on the Surface of the Catalyst*

According to the previous discussion, five different species exist on the catalysts, namely Mo in polymolybdate bulklike MoO_3 structures, Mo(VI) monolayer, Co–Mo bilayer, Co_3O_4 crystallites, and $CoAl_2O_4$. These species and their evolution with the r = Co/(Co + Mo) ratio are represented in Fig. 8. In this figure, we have not considered the $CaMoO_4$ because its content is low and its formation has an accidental character.

Naturally, the existence of such species and their amount in the catalyst will depend on the catalyst preparation method, active phase content/alumina surface area ratio, calcination temperature, and Co/(Co + Mo) ratio. Thus, for example, the use of "dry" method of impregnation and high loading, low surface and low temperature of calcination would increase the probability of formation of $CoMoO_4$ and decrease the dispersion of Co and Mo. The amount of $CoAl_2O_4$ would increase with calcination temperature and with the use of a "wet" impregnation method.

We now recall the physicochemical characteristics of these species.

—*Mo(VI) monolayer on* γ-Al_2O_3. In this monolayer Mo(VI) is present in tetrahedral environment (at low and moderate loading).

—*Mo(VI) in multilayer*. At high loading Mo(VI) is present in octahedral MoO_3 bulklike or polymolybdate environment.

—*Co–Mo bilayer on* γ-Al_2O_3. Mo(VI) is located in tetrahedral oxygen environment, Co is placed on this monolayer in octahedral oxidic surrounding as Co(III) and probably Co(II).

—$CoAl_2O_4$. This compound is formed below the Mo(VI) monolayer. Co(II) is located in tetrahedral environment, giving the typical blue color to the catalysts.

—*Aggregates of* Co_3O_4. These clusters seem to be essentially composed by Co_3O_4 in catalysts with r = 0.75–1.00.

CONCLUSION

Finally, we must state three notable consequences emerging from this work:

(i) The reduction anomaly (minimum of reducibility) observed previously (*15*) in the middle range of catalyst composition and the Co–Mo oxide interactions (*13, 14, 32, 41–44*) can be explained by the strong interaction between dispersed cobalt and molybdenum monolayer, placed as a bilayer on the surface of the catalyst.

(ii) Molybdenum monolayer improves the cobalt dispersion on the catalyst surface in catalysts prepared by the "pore volume" or "dry" impregnation (method utilized in this work).

(iii) The high performance of γ-Al_2O_3 as support in hydrodesulfurization catalysts is now evident. It enhances the molybdenum

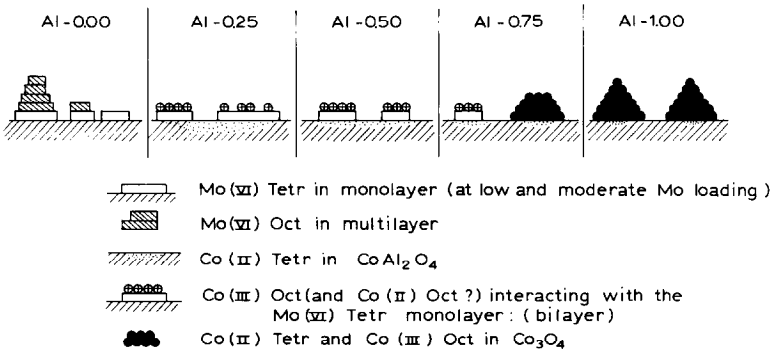

FIG. 8. Proposed structure of $CoMo/\gamma$-Al_2O_3 catalysts.

and cobalt dispersion and simultaneously the number of contacts between the cobalt and molybdenum oxide phases. The cobalt and molybdenum dispersion remains very high even after activation of catalysts (reduction–sulfidation) in hydrodesulfurization conditions (*46*).

ACKNOWLEDGMENTS

The authors gratefully acknowledge the financial support from the "Services de la Programmation de la Politique Scientifique" in the frame of the "Actions Concertées Interuniversitaires Catalyse." One of us (P.Ga.) acknowledges support from C.T.M. during the course of this investigation.

REFERENCES

1. Schuit, G. C. A., and Gates, B. C., *AIChE.* **19,** 417 (1973).
2. Hall, W. K., and Lo Jacono, M., *in* "Proceedings, 6th International Congress on Catalysis, London, 1976" (G. C. Bonds, P. B. Wells, and F. C. Tompkins, Eds.), p. 246. The Chemical Society, London, 1977.
3. Sonnemans, J., and Mars, P., *J. Catal.* **31,** 209 (1973).
4. Pott, G. T., and Stark, W. H. J., *in* "Preparation of Catalysts" (B. Delmon, P. A. Jacobs, and G. Poncelet, Eds.), p. 537. Elsevier, Amsterdam, 1976.
5. Ashley, J. H., and Mitchell, P. C. H., *J. Chem. Soc.* **A,** 2730 (1969).
6. Grimblot, J., and Bonnelle, J. P., *J. Microsc. Spectrosc. Electron.* **1,** 311 (1976).
7. Grimblot, J., Bonnelle, J. P., and Beaufils, J. P., *J. Electron Spectrosc. Relat. Phenom.* **8,** 437 (1976).
8. Tomlinson, J. R., Keeling, R. O., Rymer, G. T., and Bridges, J. M., *in* "Actes 2ème Congrès International de Catalyse," p. 1831. Editions Technip, 1961.
9. Ashley, J. H., and Mitchell, P. C. H., *J. Chem. Soc.* **A,** 2821 (1968).
10. Lipsch, J. M. J. G., and Schuit, G. C. A., *J. Catal.* **15,** 174 (1969).
11. Gour, P. K., Upadhyay, S. N., Tiwari, J. S., Ghosh, P. K., Bhattacharyya, N. B., and Sen, S. P., *J. Res. Inst. Catal. Hokkaido Univ.* **25,** 91 (1977).
12. Okamoto, Y., Nakano, H., Imanaka, T., and Teranishi, S., *Bull. Chem. Soc. Japan* **48,** 1163 (1975).
13. Grimblot, J., Pommery, J., and Beaufils, J. P., *J. Less Common Metals* **36,** 381 (1974).
14. Grimblot, J., and Bonnelle, J. P., *J. Electron Spectrosc. Relat. Phenom.* **9,** 449 (1976).
15. Garjardo, P., Grange, P., and Delmon, B., *Trans. Faraday Soc.* in press.
16. Delannay, F., Gajardo, P., Grange, P., *J. Microsc. Spectrosc. Electron.* **3,** 411 (1978).
17. Ogilvie, J. L., and Wolberg, A., *Appl. Spectra Aosc.* **26,** 401 (1972).
18. Patterson, T. A., Carver, J. C., Leyden, D. E., and Hercules, D. M., *J. Phys. Chem.* **80,** 1700 (1976).
19. Nefedov, V. I., Sergushin, N. P., Salyn, Y. V., Band, I. M., and Trzhaskovskaya, M. B., *J. Electron Spectrosc. Relat. Phenom.* **7,** 175 (1975).
20. Frost, D. C., McDowell, C. A., and Woolsey, I. S., *Mol. Phys.* **27,** 1473 (1974).
21. Borod'ko, Y. G., Vetwhinkin, S. I., Zimont, S. L., Ivleva, I. N., and Shul'ga, Y. M., *Chem. Phys. Lett.* **42,** 264 (1976).
22. Aptekar', E. L., Chudinov, M. G., Alekseev, A. M., and Krylov, O. V., *Kinet. Catal. Lett.* **1,** 493 (1974).
23. Masson, J., and Mechtschein, J., *Bull. Soc. Chim. Fr.* **10,** 3933 (1968).
24. Seshadri, K. S., and Petrakis, L., *J. Phys. Chem.* **74,** 4102 (1970).
25. Chuang, T. J., Brundle, C. R., and Rice, D. W., *Surface Sci.* **59,** 413 (1976).
26. Angevine, P. J., Delgass, W. N., and Vartuli, J. C., *in* "Proceedings, 6th International Congress on Catalysis" (G. C. Bonds, P. B. Wells, and F. C. Tompkins, Eds.). The Chemical Society, London, 1977.
27. Brinen, J. S., Schmitt, J. L., Duoghman, W. R., Achorn, P. J., Siegel, L. A., and Delgass, W. N., *J. Catal.* **40,** 295 (1977).
28. Briggs, D., *J. Electron Spectrosc. Relat. Phenom.* **9,** 487 (1976).
29. Bossi, A., Garbassi, F., and Tauszik, G. R., *J. Electron Spectrosc. Relat. Phenom.* **13,** 145 (1978).
30. Brion, D., and Escard, J., *J. Microsc. Spectrosc. Electron.* **1,** 227 (1976).
31. Brundle, C. R., *Surface Sci.* **48,** 99 (1975).
32. Martinez, N. P., Mitchell, P. C. H., and Chiplunker, P., *J. Less Common Met.* **54,** 333 (1977).
33. Praliaud, H., *J. Less Common Met.* **54,** 387 (1977).
34. Giordano, M., Bart, J. C. H., Vaghi, A., Castellan, A., and Martinotti, G., *J. Catal.* **36,** 81 (1975).
35. Asmolov, G. M., and Krylov, O. V., *Kinet. Katal.* **11,** 1028 (1970).
36. Dufaux, M., Che, M., and Naccache, C., *J. Chim. Phys. Physicochim. Biol.* **67,** 527 (1970).
37. Lo Jacono, M., Cimino, A., and Schuit, G. C. A., *Gaz. Chim. Ital.* **103,** 1281 (1973).
38. El'bert, E. I., and Tryasunov, B. G., *Kinet. Katal.* **16,** 552 (1975).
39. Asmolov, G. N., and Krylov, O. V., *Kinet. Katal.* **12,** 463 (1971).

40. Lehman, G., *J. Phys. Chem. Solids* **30,** 395 (1969).
41. Grimblot, J., D'Huydsser, A., Bonnelle, J. P., and Beaufils, J. P., *J. Electron Spectrosc. Relat. Phenom.* **6,** 71 (1957).
42. Moné, R. *in* "Preparation of catalysts" (B. Delmon, P. A. Jacobs, and G. Poncelet, Eds.), p. 381. Elsevier, Amsterdam, 1976.
43. Ishiii, Y., Nikaido, A., Matsuura, J., and Ogawa, M., *Nippon Kaguku Kaishi* **12,** 2255 (1974).
44. Okamoto, Y., Nakano, H., Shimokawa, T., Imanaka, T., and Teranishi, S., *J. Catal.* **50,** 447 (1977).
45. Brown, F. R., Tisher, R., Makovsky, L. E., and Rhee, K. H., *J. Amer. Chem. Soc. Div. Petrol. Chem.* **23 (1),** 65 (1978).
46. Gajardo, P., Mathieu, A., Grange, P., and Delmon, B., *C. R. Acad. Sci. Ser. C* **287,** 345 (1978).